ELSEVIER

Contents lists available at ScienceDirect

Carbon

journal homepage: www.elsevier.com/locate/carbon





The peculiar case of graphene growth on Co(100)

M. Jugovac ^{a,b,*}, b, I. Cojocariu ^{a,b}, C.A. Brondin ^c, V. Feyer ^d, F. Genuzio ^b, A. Locatelli ^b, T.O. Menteş ^{b,**}

- ^a Dipartimento di Fisica, Università degli studi di Trieste, Via A. Valerio 2, 34127, Trieste, Italy
- ^b Elettra Sincrotrone Trieste S.C.p.A., S.S. 14, km 163.5 in AREA Science Park, 34149, Trieste, Italy
- ^c Dipartmento di Scienze Molecolari e Nanosistemi, Università Ca' Foscari di Venezia, 30172, Venice, Italy
- ^d Peter Grünberg Institute (PGI-6), Forschungszentrum Jülich GmbH, Jülich, 52425, Germany

ARTICLE INFO

Keywords: Graphene CVD Cobalt Magnetism Symmetry Interface

ABSTRACT

Chemical vapor deposition (CVD) stands as one of the most effective methods for obtaining large-area, high-quality graphene sheets. While extensive research has focused on hexagonally symmetric substrates, there is a striking scarcity in the literature addressing graphene growth on quadratic surfaces of ferromagnetic transition metals. In this study, we devised a growth pathway of monolayer graphene on a thin Co(100) film and unraveled the electronic and magnetic properties using a combination of surface-sensitive spectro-microscopy techniques. X-ray photoemission (XPS) and angle-resolved photoemission spectroscopy (ARPES) reveal the formation of a free-standing graphene layer decoupled from the cobalt support due to the presence of a metal-carbide interlayer. Notably, high-temperature annealing transforms this decoupled graphene into a strongly interacting system, with the recrystallized cobalt assuming a hexagonal symmetry. Finally, oxygen intercalation at the Gr/C/Co(100) interface leads to the removal of the carbidic layer, forms an oxygen interlayer, which induces p-doping in the graphene layer and decouples it from the substrate.

1. Introduction

The widespread adoption of graphene in devices is hindered by the challenge of efficiently scaling up its production, making it difficult to obtain large sheets at a cost-effective rate. Over the past decade, research has shown that the CVD technique is among the most effective methods for synthesizing high-quality graphene layers at low cost [1,2]. Transition metals (TM), which are known to be excellent catalysts, have served as a platform for CVD-based graphene synthesis in numerous studies, involving, in particular, iridium [3], platinum [4], ruthenium [5], copper [6], iron [7], nickel [8] and cobalt [9]. The latter, within the TM family, has emerged as a particularly intriguing support for monolayer graphene. This has led to in-depth investigations into optimizing the structure and chemistry of graphene/cobalt composites, revealing a rich playground where the two elemental species profoundly influence the properties of one another [10–15].

The interest in the graphene/cobalt interfaces has been primarily motivated by the emergence of peculiar electronic and magnetic phenomena [10]. In particular, the presence of graphene enhances the

perpendicular magnetic anisotropy in cobalt ultrathin films and induces a sizeable Dzyaloshinskii-Moriya interaction due to an extrinsic (Rashba) spin-orbit coupling [16,17]. Moreover, recently, it has been demonstrated that this system offers a superb platform for realizing single-spin flat bands at the Fermi level by intercalating rare earth metals [11,18].

Up to now, graphene has been synthesized via CVD mainly on top of Co films with hexagonal symmetry (hcp(0001) and fcc(111)), where the relatively similar lattice constant allows for the formation of epitaxially aligned graphene [9]. While the presence of a lattice mismatch may already lead to the appearance of moiré superstructures, the stabilization of graphene on symmetry mismatched substrates leads to different moiré motifs, which may influence the electronic properties of the interface [19,20]. At the same time, the symmetry mismatch can influence the graphene growth in a profoundly different way from the symmetry-matched hexagonal surfaces. Nevertheless, graphene growth on Co(100) has not been reported yet. Indeed, the stability of surface carbides on (100) face of transition metals hinders the formation of graphene, as well as, of hBN [21,22].

E-mail addresses: matteo.jugovac@units.it (M. Jugovac), tevfik.mentes@elettra.eu (T.O. Menteş).

^{*} Corresponding author. Dipartimento di Fisica, Università degli studi di Trieste, Via A. Valerio 2, 34127, Trieste, Italy.

^{**} Corresponding author.

M. Jugovac et al. Carbon 238 (2025) 120218

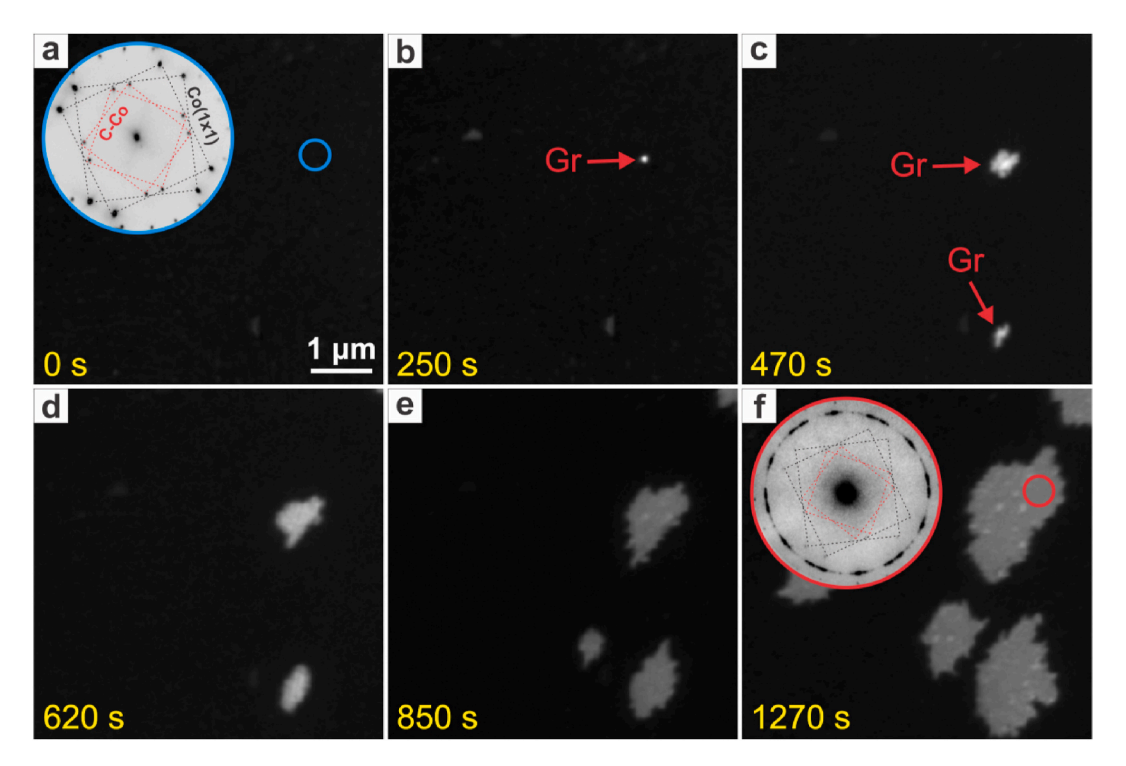


Fig. 1. Low Energy Electron Microscopy (LEEM) image sequence of the CVD growth of graphene on top of the Co(100) film at a sample temperature of 800 K while backfilling the experimental chamber with $p = 5 \times 10^{-7}$ mbar of ethylene (C_2H_4). Inset in a) shows the Low Energy Electron Diffraction (LEED) pattern ($E_k = 55$ eV) of the pristine film and in f) the one acquired on the graphene island.

In this work, we follow in real-time the CVD growth of graphene on top of thin Co(100) films deposited on carbon-reconstructed W(110) crystal and unravel the electronic and magnetic properties of the interface using a combination of surface-sensitive spectro-microscopy methods. The selection of the carbon-reconstructed tungsten is motivated by the fact that such surface acts as a template for Co(100) growth and it has a very low tendency towards Co-W intermixing [23]. The initial exposure of the Co film to ethylene, while keeping the sample at elevated temperatures, leads to carbon enrichment up to the saturation limit. Following this, graphene islands nucleate on top of a superficial cobalt-carbide layer, as revealed by synchrotron-based x-ray photoemission electron microscopy (XPEEM) at the C 1s core level. ARPES reveals that such graphene has a weak interaction with the cobalt substrate. A recrystallization procedure involving carbon dissolution and recondensation occurs if the sample is heated at around 900 K. At the same time, Co undergoes a phase transition from quadratic to hexagonal crystalline arrangement, leading graphene to be strongly bound to Co, which is metallic at the interface. Moreover, if the carbide-supported graphene is exposed to molecular oxygen at 470 K, intercalation of atomic oxygen occurs, resulting in the removal of the carbidic carbon at the interface. The prolonged intercalation process finally leads to the formation of an oxygen interlayer at the interface, remarkably modifying the electronic properties of graphene.

2. Experimental

The carbidic layer on the W(110) single crystal was obtained by exposing the clean surface to an ethylene (C_2H_4) pressure of 5×10^{-7} mbar at about 1370 K. The resulting C(15 \times 3)-W(110) reconstruction [24] was verified by Low Energy Electron Diffraction (LEED). Co was deposited on top of this surface at a rate of about 2 Å/min, using an e-beam evaporator while keeping the sample at room temperature. After the deposition of about 35 monolayers (about 6 nm), the sample was annealed up to 570 K in order to achieve a better crystalline order. Graphene growth was performed by CVD at 800 K, using ethylene as the

carbon source. Oxygen intercalation was performed while keeping the sample at 470 K in an oxygen backpressure of 5 \times 10 $^{-7}$ mbar. During all preparation and measurement steps, the base pressure was below 3 \times 10 $^{-10}$ mbar. One Langmuir (L) corresponds to an exposure of 1.33 \times 10 $^{-6}$ mbar of gas during 1 s.

The experiments were performed at the Nanospectroscopy and NanoESCA endstations of the Elettra Synchrotron in Trieste (Italy). The Low Energy Electron Microscopy (LEEM) and Diffraction (LEED), as well as X-ray Photo-Emission Electron Microscopy (XPEEM) experiments, were carried out at the Nanospectroscopy beamline using the Spectroscopic Photoemission and Low Energy Electron Microscope (SPELEEM). This instrument combines the structural information from LEEM and LEED with the chemical/magnetic sensitivity of XPEEM. The lateral resolution is around 10 nm in LEEM and 30 nm in XPEEM modes [25, 26]. The C 1s and O 1s core levels were measured using photon energies of 400 and 650 eV, respectively.

Magneto Optical Kerr Effect (MOKE) characterization was carried out in an ancillary UHV experimental chamber, which allows the exchanging of samples with the SPELEEM setup under UHV conditions without exposing the sample to ambient pressure [27]. The electromagnet of the MOKE chamber is capable of generating magnetic fields up to 140 mT. The sample can be positioned to measure either longitudinal or polar magnetic response. A CW He–Ne laser at 633 nm is used as the light source. The polarization changes are determined by the polarization-modulation technique involving a photoelastic modulator (PEM) along with lock-in methods.

The Angle-Resolved Photo Emission Spectroscopy (ARPES) experiments were carried out at the NanoESCA beamline, using a photon energy of 40 eV, p-polarization. NanoESCA endstation hosts an electrostatic PEEM equipped with a double-pass hemispherical analyzer (Focus GmBH/Omicron NanoESCA II) [28]. The instrument, in reciprocal space mode operation (k-PEEM), is capable of detecting angle (momentum)-resolved photoemission intensities simultaneously in the full-emission hemisphere above the sample surface [29]. An electron-optical column collects the photoemitted electrons, which are

M. Jugovac et al. Carbon 238 (2025) 120218

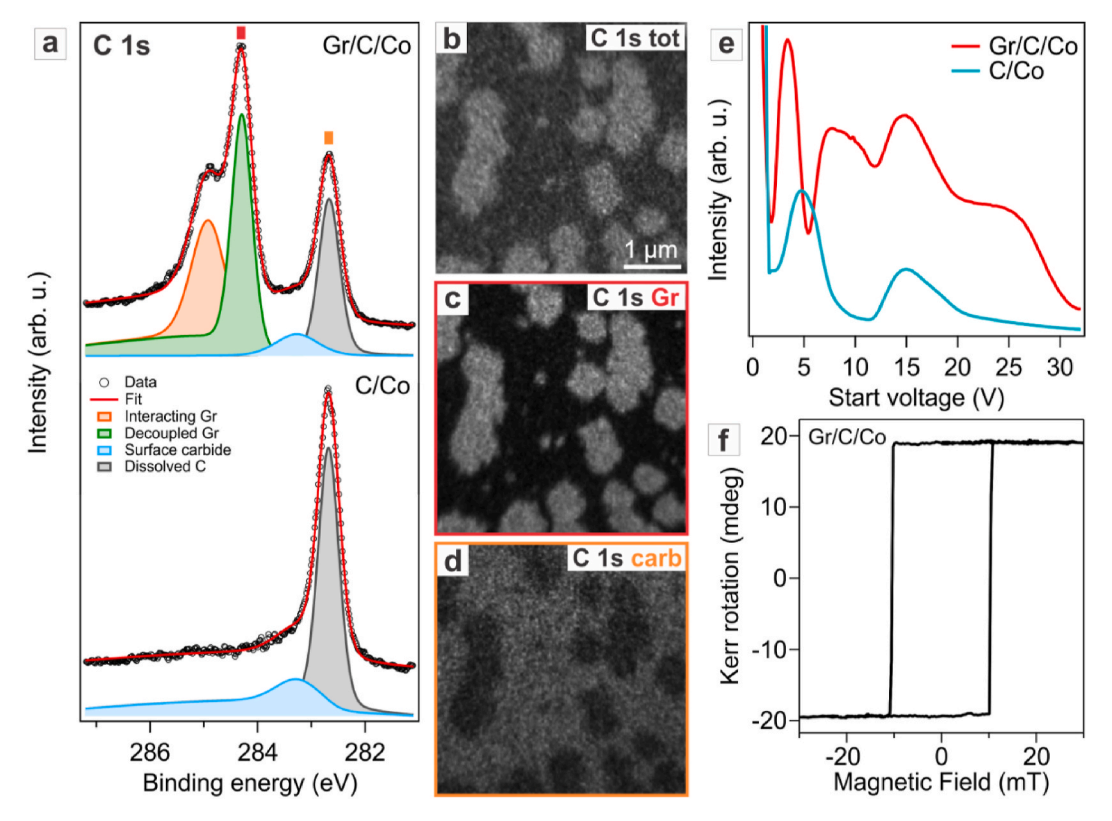


Fig. 2. a) C 1s core level for the graphene-covered (top) and uncovered regions (bottom), along with the fit. Corresponding X-ray Photo-Emission Electrom Microscopy (XPEEM) images of the total (b), graphitic (c) and carbidic (d) carbon. The images were acquired at the peaks indicated by the colored lines on the top spectrum in a). e) LEEM-IV curve of the two regions. f) Longitudinal Magneto Optical Kerr Effect (MOKE) hysteresis loop acquired on a sample with saturated graphene coverage along the W $|1\overline{10}|$ direction.

subsequently energy-filtered in the double-hemispherical configuration and finally projected onto a 2D detector. In the 2D momentum maps at selected kinetic energy, the measured parallel momentum varies in the [–2; 2] Å $^{-1}$ range. The binding energy scale was referred to the bare Co Fermi edge. From the ARPES spectra, Electron Distribution Curves (EDCs) were extracted at the $\overline{\Gamma}$ point of the surface Brillouin zone by a 0.1 Å $^{-1}$ -wide integration. These curves display the energy-dependent behavior of the band structure at selected points of the Brillouin zone.

3. Results and discussion

3.1. The growth of graphene on quadratic cobalt films

Cobalt is deposited on top of the carbon-reconstructed W(110) surface up to a thickness of 6 nm. As demonstrated previously, on top of this surface, Co adopts an fcc(100) crystalline arrangement, where the Co [011] direction coincides with the directions predetermined by the carbide structure and the cobalt lattice is dilated by 2.8 % as compared to its bulk spacing [30]. As visible from the inset of Fig. 1a, after the room-temperature deposition and subsequent mild annealing to 570 K, the Co film possesses an fcc(100) structure with two mirror domains, along with a surface c(2 \times 2) reconstruction due to surface carbon segregation [31,32].

Graphene is grown on top of the carbide-reconstructed c(2 \times 2) surface by ethylene CVD while keeping the sample at 800 K. As visible from the LEEM image sequence, the surface nucleation of graphene occurs at several surface points after about 100 L of ethylene exposure, with nanometer-sized islands (Fig. 1a–c). The islands expand along the terraces of the Co substrate (following the crystalline directions - see the $\mu\text{-LEED}$ pattern in the inset of Fig. 1a), as can be appreciated by their elongated shape upon reaching a dimension of about 1 μm (Fig. 1d). Within each island, graphene has several rotational domains, as visible

from the μ -LEED pattern in the inset of Fig. 1f acquired from a single island. Indeed, multiple arcs at a radial distance from the (00) spot compatible with first-order graphene spots can be discerned. While some preferential angles are present, no predominant azimuthal orientation can be discerned from the LEED pattern. We note that the graphene nucleation is slower as compared to the graphene synthesis on top of hcp Co(0001). Additionally, on hexagonal cobalt, graphene nucleation starts after about 40–45 L of hydrocarbon dose, while, in this case, the growth begins after a 100 L exposure. This is consistent with the higher solubility of carbon in cobalt for the fcc phase with respect to the hcp one [33].

The CVD synthesis was stopped upon reaching a graphene surface coverage of about 40 %, allowing for laterally-resolved chemical characterization of the interface using XPEEM at the C 1s core level. The surface regions not covered by graphene (Fig. 2a bottom) are characterized by a sharp peak centered at 282.7 eV and a smaller and broader component at 283.3 eV, which can be identified as the presence of surface and dissolved subsurface carbon, respectively [34], in line with previous reports on the bare Co film grown on the same substrate [31]. In the graphene-covered regions, instead, the C 1s spectrum is deconvoluted into four components, with two prominent peaks found at binding energies of 284.3 eV and 284.9 eV in addition to the same two components observed in the uncovered regions. The peak at higher binding energy is assigned to strongly interacting carbon atoms with the cobalt substrate, similar to graphene on hexagonal Co support [9,12]. Instead, the contribution at lower binding energy is tentatively assigned to carbon atoms, which weakly interact with the underlying support. This behavior can be justified either by considering that there are strongly and weakly interacting parts within the surface unit cell [35] or by considering that graphene is fully decoupled and only strongly bound at the boundaries of the nano-sized islands below the resolution limit of the microscope [36].

M. Jugovac et al. Carbon 238 (2025) 120218

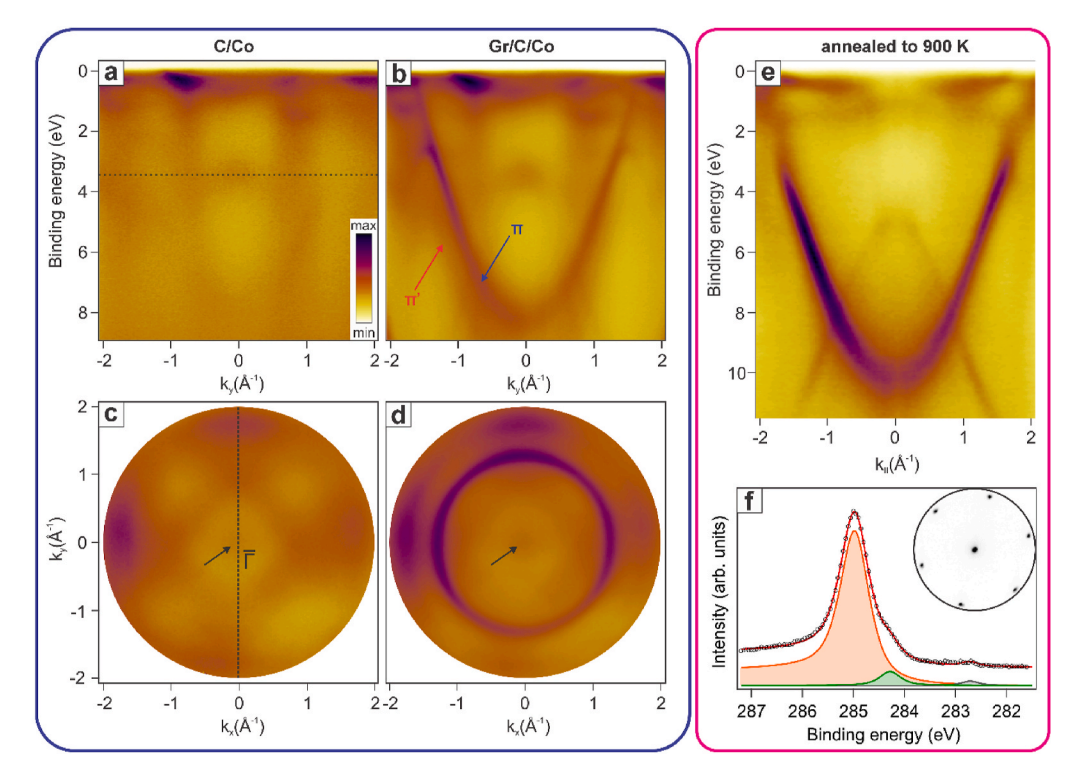


Fig. 3. ARPES-derived energy vs. momentum maps acquired along $k_x = 0$ of the C/Co substrate (a) and graphene-covered one (b). 2D momentum maps acquired at constant 3.4 eV binding energy from c) the bare substrate and d) the graphene-covered one. e) Energy vs. momentum map of the sample after annealing in UHV at 900 K. f) Corresponding C 1s core level spectrum along with the LEED pattern as an inset.

LEEM-IV spectrum acquired on the graphene islands shows two pronounced dips, as seen in Fig. 2e, which indicates the presence of an additional (ordered) layer at the interface [36]. Combined with the prominent carbidic peak in the XPS data in Fig. 2a from the graphene-covered regions, we conclude that the graphene layer is decoupled from the Co substrate with a carbidic interlayer.

The question arises regarding the magnetic state of the cobalt film, especially in the presence of bulk-dissolved carbon, which could have detrimental effects on the magnetization of the metal. Longitudinal magneto-optical Kerr effect (MOKE) hysteresis loop after growing a complete monolayer of graphene on top, a very sharp quadratic loop is observed, meaning that the cobalt film is ferromagnetic with the magnetization fully in plane, along the $[1\overline{1}0]$ crystalline direction of the tungsten substrate.

The electronic properties of the interface were analyzed using k-PEEM. The energy vs. momentum map acquired on Co(100) before graphene growth is displayed in Fig. 3a. Sharp states can be identified in the proximity of the Fermi level and are ascribed to the emission from the Co 3d bands. The energy vs. momentum map after the synthesis of monolayer graphene is visible in Fig. 3b. The sharp parabolic feature with the vertex in $\overline{\Gamma}$ (indicated by the blue arrow) is the characteristic π band of graphene. Its apex is found at 8.3 eV binding energy and is compatible with the presence of a weakly interacting graphene layer on top of cobalt, which is in agreement with previous studies [36]. In addition, a faint intensity (indicated by the red arrow) could be observed outside the main parabolic band, with a shape similar to the main π band, which is labeled as π '. This band is downshifted in energy by about 2.4 eV and agrees well with the emission from strongly interacting graphene on top of cobalt [12]. This observation aligns well with the XPS data reported in Fig. 2a, where the double-peak structure, deriving from strongly and weakly interacting carbon atoms in graphene, was observed. Nevertheless, such a large energy downshift of the Dirac point precludes any quantitative relation between C 1s binding energy and the doping level of the graphene bands [37].

In addition, by acquiring a 2D momentum map at 3.4 eV binding energy (marked as a dashed line in Fig. 3a), a pronounced intensity can be observed in the proximity of the $\overline{\Gamma}$ point (indicated by the black arrow in Fig. 3c). This feature is directly related to cobalt carbide, in line with previous reports on similar systems [38,39]. To demonstrate its origin, we grew a carbon-free Co(100) thin film on top of Cu(100), for which the carbide-related state was not observed (see Fig. S1 of the Supporting Information). Importantly, this carbidic state can also be seen upon growing graphene on the c(2x2) C/Co surface (indicated by the black arrow in Fig. 3d), confirming the presence of the carbide interlayer between the graphene and Co(100) substrate, as also deduced from the XPS and XPEEM data in Fig. 2a–d.

3.2. Conversion to hexagonal Co and carbide removal

We followed the transformations of the Gr/C/Co(100) interface via two different pathways: (i) annealing to high temperatures and (ii) exposure to molecular oxygen. By annealing the graphene-covered sample to temperatures above 900 K, the electronic structure is strongly modified (Fig. 3e). The graphene π band is shifted to higher binding energies, as seen in the momentum map data presented in Fig. 3e. The corresponding XPS peak (Fig. 3f) is located at 284.95 eV binding energy, close to the value found for the strongly-interacting graphene on Co(0001) [9]. This reflects the decomposition of the carbidic layer, in line with its reported kinetic metastability as compared to graphitic carbon on metal Co [38]. At the same time, conversion from quadratic to hexagonal crystalline arrangement occurs, as manifested by the disappearance of the Co(100)-related LEED spots and the appearance of six sharp spots arranged in a hexagonal symmetry (inset of Fig. 3f). The presence of solely six diffraction spots means that the graphene layer has its crystalline axes aligned with the those of the substrate, i.e., no rotational domains are present (as confirmed by the 2D momentum maps plotted in Fig. S3 of the Supporting Information). These observations are in line with the conversion process occurring in metallic Co films [31]. In this study, it has been determined that the

Fig. 4. a) Energy vs. momentum map acquired along $k_x = 0$ after the intercalation of oxygen at the Gr/C/Co interface. b) Electron Distribution Curve (EDC) acquired at normal emission for the bare surface, pristine Gr/C/Co, and after complete oxygen intercalation below graphene. c) C 1s core level spectrum for the Gr/C/Co interface. d) O 1s core level spectrum for the Gr/C/Co interface.

transition from fcc(100) to a film with hexagonal symmetry leads to changes in the chemical composition of the metallic film, with the dissolution of surface carbon and the presence of dissolved tungsten atoms inside the cobalt matrix. Such chemical changes were hypothesized to be the driving force for the changes in the crystal symmetry of the metal film.

In the second pathway, we exposed the Gr/C/Co(100) interface to molecular oxygen at 470 K. In the case of the graphene/cobalt interface, it was reported that oxygen intercalation occurs mainly by penetration from grain boundaries and defects into the graphene mesh [12,15]. Atomic oxygen is produced by the catalytic dissociation of molecular oxygen on graphene-free surface areas and surface defects. It then migrates along the surface and intercalates beneath the graphene layer. After the exposure, momentum maps were measured in the regions covered by graphene, and corresponding Electron Distribution Curves (EDCs) were plotted. As visible in Fig. 4a, a single graphene π and σ bands are observed with the Dirac point close to the Fermi level, indicating that the graphene is still decoupled from Co. The energy position of the band bottom is found at 7.96 eV binding energy (as noted in the EDC profile acquired at $\overline{\Gamma}$ in Fig. 4b), which is 0.31 eV lower as compared to the pristine Gr/C/Co case. This behavior is in line with the presence of oxygen at the interface, whose electron-acceptor character leads to the p-doping of the overlying graphene. In addition, the Co 3d states (found near the Fermi level as marked by the red box in Fig. 4b) are emptied due to charge transfer, as observed for oxygen intercalation at the Gr/Co (0001) interface [12]. Moreover, a remarkable change after intercalation is detected in the energy range between 3 and 4 eV binding energy. The pronounced peak, observed for the bare C/Co and Gr/C/Co and assigned to the emission from metal carbide states, vanishes after oxygen intercalation, while a small peak, corresponding to the top of the σ band is barely visible. Thus, the presence of oxygen at the interface leads to the removal of the carbidic carbon interlayer. The corresponding C 1s emission line is characterized by a single peak centered at 284.0 eV (Fig. 4c), which is characteristic of oxygen-supported graphene [12]. We emphasize that there is no evidence of trapped CO or CO2, which would manifest as an additional peak at approximately 286 eV in the C 1s photoemission spectrum [40]. Considering the limited size of the graphene islands, CO desorption is expected to occur at the island boundaries. The O 1s spectrum instead presents a single peak centered at 530.2 eV, the signature of the surface-adsorbed atomic oxygen [41].

We note that the partial intercalation of oxygen uncovers an interesting mechanism that occurs at the interface. As noted before, pristine Gr/C/Co is characterized by strongly and weakly interacting regions. In the latter, the carbide is present at the interface, while graphene is bound directly to cobalt in the former. In a partially oxygen-intercalated sample (see Fig. S4 of the Supporting Information), the electronic structure presents two distinct π bands, one characteristic of oxygen-supported graphene and the second at higher binding energies of strongly bound graphene to cobalt without a carbide interlayer. Moreover, the C 1s peak at 282.7 eV binding energy completely disappears.

This behavior suggests that the carbide layer is completely removed at the beginning of oxygen accumulation under graphene, desorbing as carbonaceous species through island boundaries.

4. Conclusion

In this study, we provide a comprehensive investigation of the CVD growth of graphene on thin ferromagnetic carbon-rich Co(100) films, offering detailed insights into the growth mechanism and interfacial chemistry. Using LEEM, we monitor the growth process in real time, showing that initial ethylene exposure leads to bulk carbon enrichment of the Co film, followed by the formation of graphene islands supported by cobalt carbide. The presence of a carbidic interlayer effectively decouples graphene from the cobalt substrate, rendering it almost freestanding. Furthermore, this decoupled graphene can be transformed into a strongly interacting one via high-temperature annealing, which also induces a phase transition in the cobalt film from quadratic to hexagonal symmetry. Additionally, the intercalation of oxygen at the graphene/ carbide/Co interface is shown to remove the carbidic layer and subsequently form an oxygen interlayer that fully decouples the graphene from the cobalt substrate and induces p-doping. Overall, our findings provide valuable insights into the growth mechanism of graphene on Co (100) films and the influence of oxygen exposure on interfacial chemistry. The ability to control the decoupling and binding of graphene to the substrate has significant implications for developing graphene-based devices and designing functional interfaces in graphene-based systems. The possibility of realizing such symmetry mismatched interfaces is even more important considering the range of crystalline arrangements present in industrially relevant metal substrates.

CRediT authorship contribution statement

M. Jugovac: Writing – review & editing, Writing – original draft, Visualization, Validation, Resources, Investigation, Formal analysis, Data curation, Conceptualization. I. Cojocariu: Writing – review & editing, Writing – original draft, Visualization, Investigation. C.A. Brondin: Writing – review & editing, Investigation. V. Feyer: Writing – review & editing, Supervision. F. Genuzio: Writing – review & editing, Investigation. A. Locatelli: Writing – review & editing, Supervision, Resources, Project administration, Investigation. T.O. Mentes: Writing – original draft, Validation, Supervision, Project administration, Investigation, Formal analysis.

Declaration of competing interest

The authors declare that they have no known competing financial interests or personal relationships that could have appeared to influence the work reported in this paper.

Acknowledgement

This work is part of the scientific activities of the CERIC–ERIC internal project MAG-ALCHEMI.

Appendix A. Supplementary data

Supplementary data to this article can be found online at https://doi.org/10.1016/j.carbon.2025.120218.

References

- B. Deng, Z. Liu, H. Peng, Toward mass production of CVD graphene films, Adv. Mater. 31 (2019) 1800996.
- [2] M. Chen, R.C. Haddon, R. Yan, E. Bekyarova, Advances in transferring chemical vapour deposition graphene: a review, Mater. Horiz. 4 (2017) 1054–1063.
- [3] J. Coraux, N. T, A. Diaye, M. Engler, C. Busse, D. Wall, N. Buckanie, F.-J. Meyer Zu Heringdorf, R. Van Gastel, B. Poelsema, T. Michely, Growth of graphene on Ir(111), New J. Phys. 11 (2009) 023006.
- [4] T. Gao, S. Xie, Y. Gao, M. Liu, Y. Chen, Y. Zhang, Z. Liu, Growth and atomic-scale characterizations of graphene on multifaceted textured Pt foils prepared by chemical vapor deposition, ACS Nano 5 (2011) 9194–9201.
- [5] S. Marchini, S. Günther, J. Wintterlin, Scanning tunneling microscopy of graphene on Ru(0001), Phys. Rev. B 76 (2007) 075429.
- [6] C. Mattevi, H. Kim, M. Chhowalla, A review of chemical vapour deposition of graphene on copper, J. Mater. Chem. 21 (2011) 3324–3334.
- [7] H. An, W.-J. Lee, J. Jung, Graphene synthesis on Fe foil using thermal CVD, Curr. Appl. Phys. 11 (2011). S81–5.
- [8] L.L. Patera, C. Africh, R.S. Weatherup, R. Blume, S. Bhardwaj, C. Castellarin-Cudia, A. Knop-Gericke, R. Schloegl, G. Comelli, S. Hofmann, C. Cepek, *In situ* observations of the atomistic mechanisms of Ni catalyzed low temperature graphene growth, ACS Nano 7 (2013) 7901–7912.
- [9] M. Jugovac, F. Genuzio, E. Gonzalez Lazo, N. Stojić, G. Zamborlini, V. Feyer, T. O. Mentes, A. Locatelli, C.M. Schneider, Role of carbon dissolution and recondensation in graphene epitaxial alignment on cobalt, Carbon 152 (2019) 489-496
- [10] M. Jugovac, E.D. Donkor, P. Moras, I. Cojocariu, F. Genuzio, G. Zamborlini, G. Di Santo, L. Petaccia, N. Stojić, V. Feyer, C.M. Schneider, A. Locatelli, T.O. Mentes, Spin-polarized hybrid states in epitaxially-aligned and rotated graphene on cobalt, Carbon 198 (2022) 188–194.
- [11] M. Jugovac, I. Cojocariu, V. Feyer, S. Blügel, G. Bihlmayer, P. Perna, Spin-dependent electronic phenomena in heavily-doped monolayer graphene, Carbon 119666 (2024).
- [12] M. Jugovac, F. Genuzio, T.O. Menteş, A. Locatelli, G. Zamborlini, V. Feyer, C. M. Schneider, Tunable coupling by means of oxygen intercalation and removal at the strongly interacting graphene/cobalt interface, Carbon 163 (2020) 341–347.
- [13] M. Jugovac, C. Tresca, I. Cojocariu, G. Di Santo, W. Zhao, L. Petaccia, P. Moras, G. Profeta, F. Bisti, Clarifying the apparent flattening of the graphene band near the van Hove singularity, Phys. Rev. B 105 (2022) L241107.
- [14] J. Hwang, C. Hwang, N.-K. Chung, A.D. N'Diaye, A.K. Schmid, J. Denlinger, The hybridizations of cobalt 3d bands with the electron band structure of the graphene/ cobalt interface on a tungsten substrate, J. Kor. Phys. Soc. 69 (2016) 573–577.
- [15] V.O. Shevelev, K.A. Bokai, A.A. Makarova, D. Marchenko, Vilkov O. Yu, Mikhailovskii V. Yu, D.V. Vyalikh, D Yu Usachov, Highly ordered and polycrystalline graphene on Co(0001) intercalated by oxygen, J. Phys. Chem. C 124 (2020) 17103–17110.
- [16] H. Yang, G. Chen, A.A.C. Cotta, A.T. N'Diaye, S.A. Nikolaev, E.A. Soares, W.A. A. Macedo, K. Liu, A.K. Schmid, A. Fert, M. Chshiev, Significant Dzyaloshinskii–Moriya interaction at graphene–ferromagnet interfaces due to the Rashba effect, Nat. Mater. 17 (2018) 605–609.
- [17] F. Ajejas, A. Gudín, R. Guerrero, A. Anadón Barcelona, J.M. Diez, L. de Melo Costa, P. Olleros, M.A. Niño, S. Pizzini, J. Vogel, M. Valvidares, P. Gargiani, M. Cabero, M. Varela, J. Camarero, R. Miranda, P. Perna, Unraveling dzyaloshinskii-moriya interaction and chiral nature of graphene/cobalt interface, Nano Lett. 18 (2018) 5364–5372.
- [18] M. Jugovac, I. Cojocariu, J. Sánchez-Barriga, P. Gargiani, M. Valvidares, V. Feyer, S. Blügel, G. Bihlmayer, P. Perna, Inducing single spin-polarized flat bands in monolayer graphene, Adv. Mater. 35 (2023) 2301441.

- [19] A. Sala, Z. Zou, V. Carnevali, M. Panighel, F. Genuzio, T.O. Menteş, A. Locatelli, C. Cepek, M. Peressi, G. Comelli, C. Africh, Quantum confinement in aligned zigzag "pseudo-ribbons" embedded in graphene on Ni(100), Adv. Funct. Mater. 32 (2022) 2105844.
- [20] Z. Zou, V. Carnevali, M. Jugovac, L.L. Patera, A. Sala, M. Panighel, C. Cepek, G. Soldano, M.M. Mariscal, M. Peressi, G. Comelli, C. Africh, Graphene on nickel (100) micrograins: modulating the interface interaction by extended moiré superstructures, Carbon 130 (2018) 441–447.
- [21] K. Takahashi, K. Yamada, H. Kato, H. Hibino, Y. Homma, In situ scanning electron microscopy of graphene growth on polycrystalline Ni substrate, Surf. Sci. 606 (2012) 728–732.
- [22] S. Suzuki, R. Molto Pallares, C.M. Orofeo, H. Hibino, Boron nitride growth on metal foil using solid sources, Journal of Vacuum Science & Technology B, Nanotechnology and Microelectronics: Materials, Processing, Measurement, and Phenomena 31 (2013) 041804.
- [23] A. Christensen, A.V. Ruban, P. Stoltze, K.W. Jacobsen, H.L. Skriver, J.K. Nørskov, F. Besenbacher, Phase diagrams for surface alloys, Phys. Rev. B 56 (1997) 5822–5834
- [24] A. Varykhalov, O. Rader, W. Gudat, Structure and quantum-size effects in a surface carbide: W (110) / C R (15 \times 3), Phys. Rev. B 72 (2005) 115440.
- [25] A. Locatelli, L. Aballe, T.O. Mentes, M. Kiskinova, E. Bauer, Photoemission electron microscopy with chemical sensitivity: SPELEEM methods and applications, Surf. Interface Anal. 38 (2006) 1554–1557.
- [26] T.O. Mentes, G. Zamborlini, A. Sala, A. Locatelli, Cathode lens spectromicroscopy: methodology and applications, Beilstein J. Nanotechnol. 5 (2014) 1873–1886.
- [27] F. Genuzio, T. Giela, M. Lucian, T.O. Mentes, C.A. Brondin, G. Cautero, P. Mazalski, S. Bonetti, J. Korecki, A. Locatelli, A UHV MOKE magnetometer complementing XMCD-PEEM at the Elettra Synchrotron, J. Synchrotron Radiat. 28 (2021) 995–1005.
- [28] C. Wiemann, M. Patt, I.P. Krug, N.B. Weber, M. Escher, M. Merkel, C.M. Schneider, A new nanospectroscopy tool with synchrotron radiation: NanoESCA@Elettra, e-J. Surf. Sci. Nanotechnol 9 (2011) 395–399.
- [29] G. Zamborlini, M. Jugovac, I. Cojocariu, D. Baranowski, S. Mearini, Y.Y. Grisan Qiu, V. Feyer, C.M. Schneider, Exploring spin- and momentum-resolved phenomena at the NanoESCA beamline of Elettra synchrotron, Synchrotron Radiat. News 1–6 (2024).
- [30] H. Pinkvos, H. Poppa, E. Bauer, J. Hurst, Spin-polarized low-energy electron microscopy study of the magnetic microstructure of ultra-thin epitaxial cobalt films on W(110), Ultramicroscopy 47 (1992) 339–345.
- [31] M. Jugovac, I. Cojocariu, F. Genuzio, C.A. Brondin, V. Feyer, C.M. Schneider, A. Locatelli, T.O. Mentes, Thermally induced chemical and structural transformations in thin cobalt films, ACS Appl. Electron. Mater. 6 (2024) 5050–5056.
- [32] A. Bettac, J. Bansmann, V. Senz, K.H. Meiwes-Broer, Structure and magnetism of hcp(0001) and fcc(001) thin cobalt films on a clean and carbon-reconstructed W (110) surface, Surf. Sci. 454–456 (2000) 936–941.
- [33] K. Ishida, T. Nishizawa, The C-Co(Carbon-Cobalt) system, JPE 12 (1991) 417–424.
- [34] R. Gubo, P. Ren, X. Yu, T. Zhang, X. Wen, Y. Yang, Y.-W. Li, J.W. Hans Niemantsverdriet, C.J. Kees-Jan Weststrate, Similarities and trends in adsorbate induced reconstruction – structure and stability of FCC iron and cobalt surface carbides. Appl. Surf. Sci. 626 (2023) 157245.
- [35] A.B. Preobrajenski, M.L. Ng, A.S. Vinogradov, N. Mårtensson, Controlling graphene corrugation on lattice-mismatched substrates, Phys. Rev. B 78 (2008) 073401.
- [36] M. Jugovac, I. Cojocariu, F. Genuzio, C. Bigi, D. Mondal, I. Vobornik, J. Fujii, P. Moras, V. Feyer, A. Locatelli, T.O. Mentes, Effect of residual carbon on spinpolarized coupling at a graphene/ferromagnet interface, Adv Elect Materials 9 (2023) 2300031.
- [37] U.A. Schröder, M. Petrović, T. Gerber, A.J. Martínez-Galera, E. Grånäs, M. A. Arman, C. Herbig, J. Schnadt, M. Kralj, J. Knudsen, T. Michely, Core level shifts of intercalated graphene, 2D Mater. 4 (2016) 015013.
- [38] Y.-H. Zhao, H.-Y. Su, K. Sun, J. Liu, W.-X. Li, Structural and electronic properties of cobalt carbide Co2C and its surface stability: density functional theory study, Surf. Sci. 606 (2012) 598–604.
- [39] Z. Yang, T. Zhao, S. Hao, R. Wang, C. Zhu, Y. Tang, C. Guo, J. Liu, X. Wen, F. Wang, Large-scale synthesis of multifunctional single-phase Co₂ C nanomaterials, Adv. Sci. 10 (2023) 2301073.
- [40] Puppo S. Del, V. Carnevali, D. Perilli, F. Zarabara, A.L. Rizzini, G. Fornasier, E. Zupanič, S. Fiori, L.L. Patera, M. Panighel, S. Bhardwaj, Z. Zou, G. Comelli, C. Africh, C. Cepek, C. Di Valentin, M. Peressi, Tuning graphene doping by carbon monoxide intercalation at the Ni(111) interface, Carbon 176 (2021) 253–261.
- [41] J. Nakamura, I. Toyoshima, K. Tanaka, Formation of carbidic and graphite carbon from CO on polycrystalline cobalt, Surf. Sci. 201 (1988) 185–194.